Combinatorial engineering of bulk-assembled monodisperse coacervate droplets towards logically integrated protocells

Qingchuan Li[1, 2, #, *], Qingchun Song[2, #], Jing Wei[1], Yang Cao[2], Dairong Chen[1, *], Ho Cheung Shum[2, *]

[1]School of Chemistry & Chemical Engineering, National Engineering Research Center for Colloidal Materials, Shandong University, Jinan 250100, P. R. China.
[2]Department of Mechanical Engineering, The University of Hong Kong, Pokfulam Road, Hong Kong, China

*Correspondence to: ashum@hku.hk; cdr@sdu.edu.cn; lqc3038@hku.hk
[#]These authors contributed equally to this work

Abstract. The emergence of life requires the appropriate integration of protometabolisms, compartments, and protogenomes from an intricate interplay of non-living constituents. Unveiling the mechanism of how life-related building blocks are logically integrated towards life from a high diversity of inanimate matter is an ongoing challenging task of current science. Various compartments such as lipid vesicles and coacervates have been proposed as possible microcontainers to hold prebiotic genetic materials and metabolic reactions for the construction of integrated systems. However, the spontaneous assembly of these compartments allows no selective and logical integration from a high diversity of inanimate matter, thus making the appropriate integration of the inanimate towards membranous life more a coincident and low probability event. Herein, we show that the assembly of colloidal particles with coacervate-forming molecules provides a combinatorial approach for the regularization of matter of chaos towards protocells with cellular hallmarks of size uniformity, logical integration, and unilamellar membransation. Monodisperse coacervate droplets coated by colloidal particles are assembled through hydrodynamic forcing-promoted coalescence. Using these coacervates as platform, a combinatorially integrative approach is developed to engineer the complexity of coacervates, from coacervate entities with programmable spatial loading to diverse interconnected coacervate consortia with collective morphology evolution. A fluidic unilamellar membrane is assembled on coacervate via freeze-thaw treatment of coacervates coated by liposome particles, including liposome particles with heterogenous lamellarity, resulting in coacervate-supported monodisperse giant unilamellar vesicles with gated permeability to polar molecules and remarkable structural and functional stability at extreme environments. This work provides an integrative approach to process crude building blocks towards disciplined and integrated cellular systems, which might have mediated the transition from the inanimate to life. This approach is promisingly utilized for high throughput screening of possible integrated form of primitive life from a high diversity of inanimate matter as well as on demand bulk-generation of monodisperse hierarchical microdroplets with flexibly integrated functions.

Introduction

It is generally accepted that living being must possess appropriately integrated essential properties of replication, metabolism, and compartmentalisation[1]. The mechanism of how the first integration of these three essential properties towards life is enabled from a high diversity of inanimate matter is an ongoing debate[2-4]. From the perspective of matter assembly, this integration can be deem to the proper interplay of specific non-living constituents towards minimum living systems[5]. Therefore, a prebiotically plausible integrative approach that allows logical integration from the multitudinous inanimate matter might address the transition from the inanimate to life. Nature provides various crude compartments such as lipid vesicles[6-8] and coacervates[9,10] to serve as prebiotic containers for life-related building blocks. Among them, lipid vesicles are predominantly used due to their structual similarity to the cell envelope of contempory cellular life[11,12]. However, the spontaneous assembly of most lipids generally results in lipid vesicles with heterogenous lamellarity and low molecule encapsulation efficiency[13,14]. It is still unknown how nature has processed these lipid vesicles with heterogenous lamellarity towards unilamellar membrane feature of most modern cells. Moreover, the low molecule encapsulation efficiency during lipid self-assembly makes the proper integration of essential building blocks towards life an extremely low probability event.

As a candiate, coacervate droplet composing high concentration of associated organic molecules exhibits robust ability to concentrate life-related building blocks[15]. Coacervates were hypothesized to have provided chemical reaction centres during the early steps in the origin of life[16], which is further strengthened by the recent discovery of coacervates in cells as important membraneless organelles[17,18]. However, coacervates are dynamic systems, exhibiting active assembly and disassembly, prone to fuse, and allowing molecule exchange among coacervates[9,19]. Therefore, they fail to provide a stable compartment for specialized cargo loading among coacervates. Moreover, a robust mechanism for the evolution of coacervates towards modern life with a fluidic unilamellar membrane is demanded. Pioneering efforts have been made to form lipid vesicles with heterogeneous lamellarity from coacervates by using coacervate as the scaffold for amphiphilic molecules assembly[10] or expoiting a coacervate-to-vesicle transition mechanism[20]. A prebiotically plausible mechanism enabling evolution of coacervates towards the fluidic unilamellar membrane hallmark of modern cell envelope with cellular size uniformity remains to be explored.

Thereout, although nature has provided multifold thermodynamics-favorable possible compartments to nurture primitive life, revisting a mechanism allowing the processing these crude assemblies towards minimum living systems with logically integrated essential building blocks is still among the grand challenges of contemporary science. Colloidal particles such as mineral particles and vesicles have been proposed to be important constituents of primordial soup intimately associated with synthesis of life-related building blocks and catalysis for metabolic reactions[1]. Herein, through the co-assembly of model colloidal particles with coacervate-forming molecules, this work demonstrated a prebiotically plausible integrative approach that can combinatorially sculpt the random colloidal primordial soup into protocell models with cellular hallmarks of size uniformity, logical integration, and unilamellar fluidic membransation. This approach represented a way to process crude building blocks towards disciplined and logically integrated protocellular systems.

Results and Discussion

Formation of monodisperse coacervates stabilized by colloidal particles. A vortex assisted co-

assembly method was employed to assemble poly(diallyldimethylammonium chloride) (PDDA) and adenosine 5′-triphosphate (ATP) with different colloidal particles. PDDA and colloidal particles were firstly mixed, and then subsequently with ATP via vortex for 30 s. Depending on [PDDA] and [ATP] ratio φ and particle type, four cases were observed in the assembly results (Figs. 1a, b and S1, 2), namely, polydisperse coacervates with particles outside (Case 1), at interface (Case 2), or inside (Case 3), and monodisperse coacervates interfacially stabilized by particle layer (Case 4). The former three cases were previously observed in Mann, Hest and Keating's studies of coacervates interacting with inorganic nanoparticles[21], chloroplast[22], liposomes[23], and polymersomes[24]. However, the bulk assembly of monodisperse coacervates shown in case 4 is reported for the first time. Various nanoparticles, including liposomes of various membrane compositions, silica particles coated by lipid bilayer, magnetic nanoparticles, and polystyrene (PS) particles with different surface groups, are shown to be able to assemble with PDDA and ATP to form monodisperse coacervates (Fig. 1b and S3). PDDA-ATP coacervate coated with 100 nm 1,2-dioleoyl-*sn*-glycero-3-phosphocholine (DOPC)/1,2-dioleoyl-*sn*-glycero-3-phospho-L-serine (sodium salt) (DOPS) liposomes (Molecular percentage of DOPS χ = 10%) is taken as an example to check the stability of coacervates and the feasibility for size control. No obvious variation of average diameter and morphology was observed in three days at 4°C, which verified the stability, as shown in Fig. S4. The diameter of the coacervates was controlled by varying the amount of liposomes used. As the liposome concentration increases from 0.025 mg/mL to 0.20 mg/mL, the coacervate diameter decreases from ~20 μm to 2 μm (Fig. S5).

Mechanism of monodisperse coacervates formation. To elucidate the mechanisms for the different partitioning behaviors of particles across the coacervates and monodisperse coacervate formation, we use liposome as model particle and investigate the influence of liposome composition and [PDDA]/[ATP] ratio φ on coacervate formation. The φ and DOPS percentage χ in DOPC/DOPS liposomes affect the formation of coacervates into the four cases in Fig. 1a, as indicated by the phase diagram in Fig. 1c. With an increase of φ or χ, liposomes display a partition tendency from the dilute phase (Case 1) to the interface (Case 2 and 4), and then to the coacervate phase (Case 3). Monodisperse coacervates are generated at χ value from 5% to 12% at specific φ range. With increasing χ, the range of φ shifts to a lower φ value.

Based on the results in Fig. 1c, we propose an interfacial tension determined partitioning mechanism for charged particles in coacervate system (Fig. 1d). A charged particle in the coacervate system is considered to exist as a complex comprising particle and adsorbed charged polymers. An interfacial tension $\gamma_{p\text{-}d}$ between particle-polymer complex and dilute phase appears because of particle-polymer charge complexation[25]. Analogous to particle partitioning in oil-water and aqueous two phase systems[26,27], the partitioning behavior of the particle-polymer complex is a result of the balance among $\gamma_{p\text{-}d}$, coacervate phase-dilute phase interfacial tension $\gamma_{c\text{-}d}$ and particle-coacervate phase interfacial tension $\gamma_{p\text{-}c}$. The particle located in dilute phase when $\gamma_{p\text{-}c}>\gamma_{p\text{-}d}+\gamma_{c\text{-}d}$ and in coacervate phase when $\gamma_{p\text{-}d}>\gamma_{p\text{-}c}+\gamma_{c\text{-}d}$. A contact angle θ with $\cos\theta=(\gamma_{p\text{-}c}-\gamma_{p\text{-}d})/\gamma_{c\text{-}d}$ is expected when the particle-polymer complex located at coacervate surface. With reference to Fig. 1c, an increase of χ would represent a strengthening of the association between liposome and PDDA, while an increase of φ would induce more PDDA adsorption, thereby resulting in an increase of $\gamma_{p\text{-}d}$. Therefore, with the increase of χ and φ, the increased $\gamma_{p\text{-}d}$ induces the partition of liposomes from dilute phase to interface, and to coacervate phase. Based on the above mechanism, the zeta potential ζ of different

charged colloidal particles should play a determining role in particle partitioning behavior. We test this hypothesis by characterizing the partitioning behaviors of PDDA-ATP coacervates (φ=3/2) of different charged particles with diameter ranging from 30 nm to 100 nm. Particles with $|\zeta|$ below 10 mV, between 10 mV to 40 mV, or above 40 mV preferentially locate in the dilute phase, interface, or coacervate phase, respectively, in agreement with our hypothesis. The interfacial tension driven partitioning behavior arising from particle-polymer association might account for the various cargo recruitment behaviors in synthetic coacervates[21,23] and biomolecular condensates[28]. For instance, negatively charged lipids were reported to be necessary for the recruiment of vesicles in synapsin condensates[28]. Besides, this mechanism built the foundation for the engineering of particle partitioning via tailoring particle surface properties. 100 nm silica particles with ζ of -52.3±4.1 mV positioned in the coacervate phase when assembled with PDDA and ATP (Fig. S2). However, when coated with DOPC/DOPS (χ=7.5% or 10%) lipid bilayer, their location would shift to the coacervate surface, leading to formation monodisperse coacervates (Fig. S3). Another consequence of this mechanism is the denser packing of particles at coacervate surface with increased particle charges (Fig.S6), contrary to previous reports for charged particle assembly at oil-water interface[29,30]. Particles with more charges associate stronger with polymers, resulting in higher $\gamma_{p\text{-}d}$. The hydrophobic interaction among particles drove denser particle packing according to modified Derjaguin–Landau–Verwey–Overbeek theory[31].

A limited coalescence process promoted by vortexing is considered to acount for the formation of particle coated monodisperse PDDA-ATP coacervates (Fig. 1f). Small coacervates with particles on surface are firstly formed upon mixing of PDDA, particles and ATP. Because of the large specific surface area of these initially formed small coacervates, the particle coverage is too low to provide enough protection against coalescence. Therefore, driven by $\gamma_{c\text{-}d}$, these coacervates tend to coalesce under vortex, consequently reducing the coacervate specific surface area and increasing particle packing. Metastable coacervates are generated when the particle layer provided enough steric hindrance and repulsive electrostatic energy against further coalescence. The monodispersity of these particle-coated coacervates depended on φ, particle charges, and formation method (vortex or gentle incubation). φ and particle charges influenced the contact angle θ of particles on coacervate surface. To generate monodisperse coacervates, θ should be <90° but large enough to avoid particle desorption during coalescence process. Comparing the vortexing and gentle incubation method (Fig. S7), vortexing promotes collision of the coacervates and overcomes the resistance of electrostatic repulsive forces among coacervates against coalescence, thus resulting in the formation of coacervates with remarkable monodispersity (Polydispersity index <0.02) in 30 s (Fig. 1g).

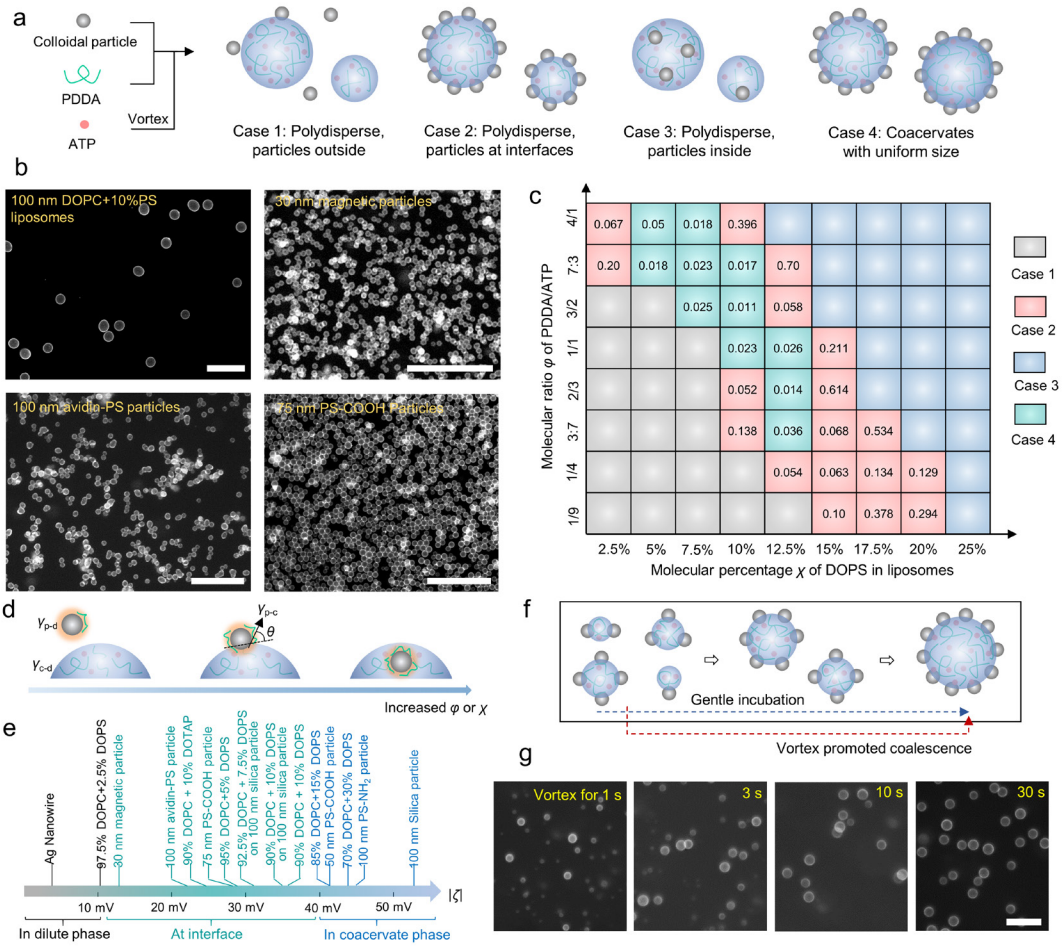

Figure 1. Formation of monodisperse PDDA-ATP coacervates coated by colloidal particles. a, schematic showing four cases of assembly observed by mixing PDDA and colloidal particles firstly and subsequently with ATP via vortex. **b**, fluorescence images of monodisperse coacervates coated by 100 nm DOPC/DOPS liposomes (Molecular percentage of DOPS χ = 10%), 30 nm magnetic nanoparticles, 100 nm streptavidin-coated PS particles, or 75 nm PS-COOH particles. [PDDA]+[ATP] concentration in the final mixture was 5 mM. Molecular ratio of PDDA/ATP φ in the four colloids-coacervate systems were respectively 13:7, 1:1, 3:2, and 3:2. Colloids concentration were respectively 0.05, 0.035, 0.10, and 0.05 mg/mL. **c**, Phase diagram for the assembly results in DOPC/DOPS liposome-PDDA-ATP system at different χ and φ. The values in the table were the calculated polydispersity index from at least 100 coacervates for each case. Coacervate dispersion with polydispersity index ≤ 0.05 was considered as monodisperse. **d**, Schematic illustrating the mechanism of liposome partitioning across the coacervate controlled by φ and χ. **e**, Positioning behavior of colloidal particles of different compositions and zeta potential $|\zeta|$ across PDDA-ATP coacervates (φ=3/2). **f**, Schematic showing the formation process of coacervates coated by colloidal particles via gentle incubation or vortex assisted coalescence. **g**, fluorescence images of the PDDA-ATP (φ=3/2) coacervates coated by DOPC/DOPS (χ = 10%) liposomes by vortexing for different time. Liposome concentration was 0.03 mg/mL. The scales bars in **b** and **g** were respectively 50 μm and 20 μm.

Monodisperse coacervate formation from other charged species. To validate the versatility of this method to generate monodisperse coacervates with different components, DOPC/DOPS liposomes are used as model particles for co-assembly with another four cationic specie-anionic specie pairs, namely, PDDA with two anionic species, adenosine diphosphate (ADP) and polyacrylic acid (PAA), and ATP with two cationic species, polyallylamine (PAH) and polyethyleneimine (PEI).

These four pairs represent typical examples with different degree of charge association in comparison with PDDA-ATP, following PDDA-PAA>PDDA-ATP>PDDA-ADP and PAH-ATP>PEI-ATP>PDDA-ATP at neutal pH condition (Fig. 2).

Monodisperse coacervates can be generated in all four different systems but under different conditions. In the PDDA-ADP system, monodisperse coacervates are generated at low χ value of 2.5% with φ (PDDA/ADP) ranging from 1/4 to 3/7 (Fig. 2a). In the PDDA-PAA system, no coacervates are formed in the absence of salt. Monodisperse PDDA-PAA coacervates coated by DOPC/DOPS (χ=50%) liposomes are obtained with NaCl concentration above 100 mM and φ (PDDA/PAA) range of 1/4 to 3/7 (Fig. 2b). In PAH-ATP and PEI-ATP systems,monodisperse coacervates are formed at alkaline pH condition when assembled with DOPC/DOPS (χ=10%) liposomes (Fig. 2b, c). Monodisperse PAH-ATP coacervates are formed at pH=8.8 and φ (PAH/ATP) range of 8/3 to 4/1 (Fig. 2b). PEI-ATP system needed a relative lower alkaline pH value from 7.3 to 7.7 and φ (PAH/ATP) range of 7/3 to 4/1 to generate monodisperse coacervates (Fig. 2c). The different requirements for the formation of monodisperse coacervates with different components can be explained by a balance among $\gamma_{p\text{-}c}$, $\gamma_{p\text{-}d}$ and $\gamma_{c\text{-}d}$, as shown in Fig.1d. For example, ADP was more weakly associated with PDDA than ATP, which resulted in smaller $\gamma_{c\text{-}d}$. Therefore, to avoid partitioning of liposomes in coacervate phase ($\gamma_{p\text{-}d}>\gamma_{p\text{-}c}+\gamma_{c\text{-}d}$), liposomes with low χ value of 2.5% that provide small $\gamma_{p\text{-}d}$ are used to stabilize coacervates (Fig. 2a). In contrast, with the more strongly associated PDDA-PAA, PAH-ATP and PEI-ATP systems (Larger $\gamma_{c\text{-}d}$), salt concentration or pH value need to be modulated to reduce $\gamma_{c\text{-}d}$ or liposomes with higher χ are needed to increase $\gamma_{p\text{-}d}$ for monodisperse coacervates formation.

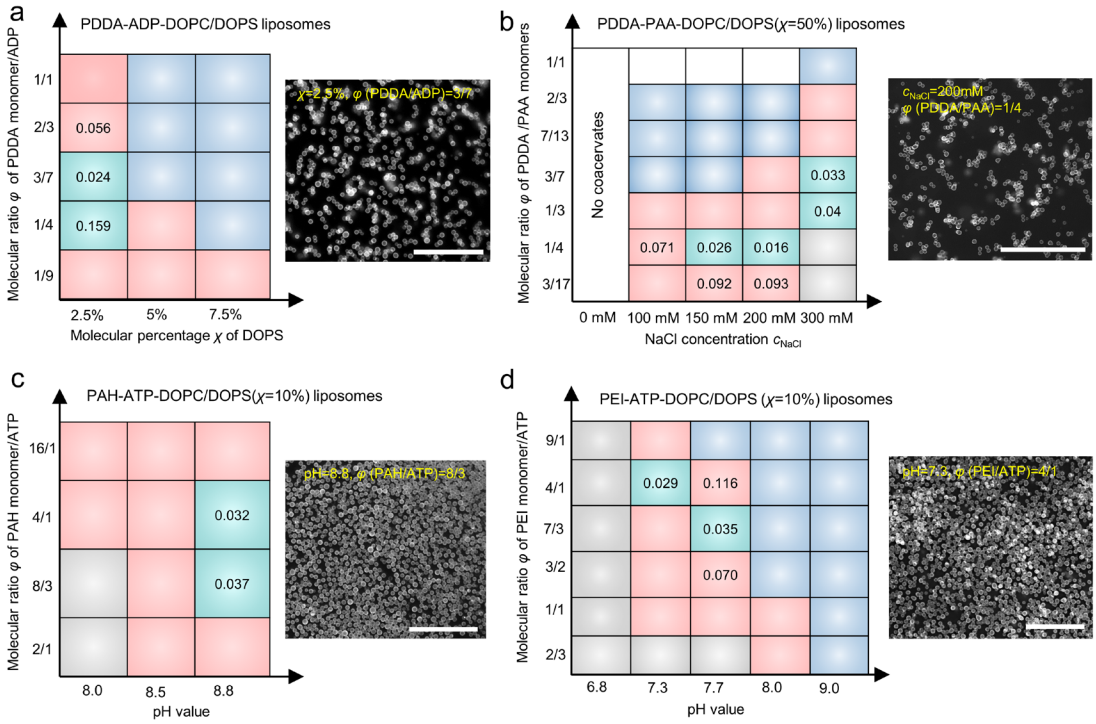

Figure 2. Formation of monodisperse coacervates from other charged species. a, Phase diagram showing the influence of χ and [PDDA]/[ADP] ratio on coacervate formation. [PDDA]+[ADP] was 5 mM. Liposome concentration was 0.10 mg/mL. **b**, Phase diagram showing the influence of NaCl concentration and [PDDA]/[PAA] ratio on coacervates formation with the existence of DOPC/DOPS (χ=50%) liposomes. [PDDA]+[PAA] was 20 mM. Liposome concentration was 0.10 mg/mL. **c**, Phase diagram showing the influence of pH value and [PAH]/[ATP]

ratio on coacervate formation with existence of DOPC/DOPS (χ=10%) liposomes. [PAH]+[ATP] was 25 mM. Liposome concentration was 0.10 mg/mL. **d**, Phase diagram showing the influence of pH value and [PEI]/[ATP] ratio on coacervate formation with the existence of DOPC/DOPS (χ=10%) liposomes. [PEI]+[ATP] was 10 mM. Liposome concentration was 0.05 mg/mL. The fluorescence images were the typical images of the monodisperse coacervates. The scales bars were 50 μm.

Hierarchical coacervates via combinatorial fusion. Very small unstable coacervates were firstly formed when particles and counter-charged species were just mixed, which took more than 30 min for them to fuse into metastable coacervates through gentle incubation, but only 30 s via vortexing, as shown in Fig. 1f, g and S7. This difference implies the potential to engineer the hierarchical coacervates via combinatorial fusion. A series of small unstable coacervates with various structures were first formed via the gentle mixing of particles and counter-charged species. These small coacervates are then taken as building blocks to generate hierarchical coacervates with elaborately engineered structures via vortex-assisted fusion of selected building blocks.

Nine types of coacervate building blocks (1)-(9) are designed by gently mixing PDDA, ATP, liposomes with red (R-liposome) or green (G-liposome) fluorescence, PAH, or PS particles with blue (B-PS particle) or green (G-PS particle) fluorescence. Through the self- or mutual fusion of these building blocks via vortexing, the surface and inner compartment of the coacervates can be elaborately engineered. On PDDA-ATP coacervate surface, we control the spatial organization of R-liposome and G-liposome, including the heterogeneously distributed configuration comprising microsized patches of different liposomes (Fig. 3b and S8) and homogeneous liposome mixing (Fig. 3c). Inside PDDA-ATP coacervates, the homogeneous or heterogenous spatial organization of one or two objects is delicately controlled (Fig. 3d-g). Multiphase coacervates composed of PDDA-ATP rich phase and PAH-ATP rich phase (Fig. 3h and S9) are generated via the vortex-assisted self-fusion of coacervate building blocks (7); the resultant morphology bears resemblance to those of eukaryotic cells with inner phase as nucleus and outer phase as cytoplasm. An even higher degree of complexity can be introduced into these multiphase coacervates by spatial loading of B-PS particle or G-PS particle in PDDA-ATP-rich phase as “organelles” (Fig. 3i-j) through the self-fusion of building blocks (8) or (9). This combinatorial fusion approach provides a route for on-demand generation of programmable coacervates with desired hierarchical structures. From the perspective of the origin of life, the combinatorial fusion process could have enabled integration of different life-related building blocks or metabolic processes into a single compartment, providing a basis for the initiation of primitive life.

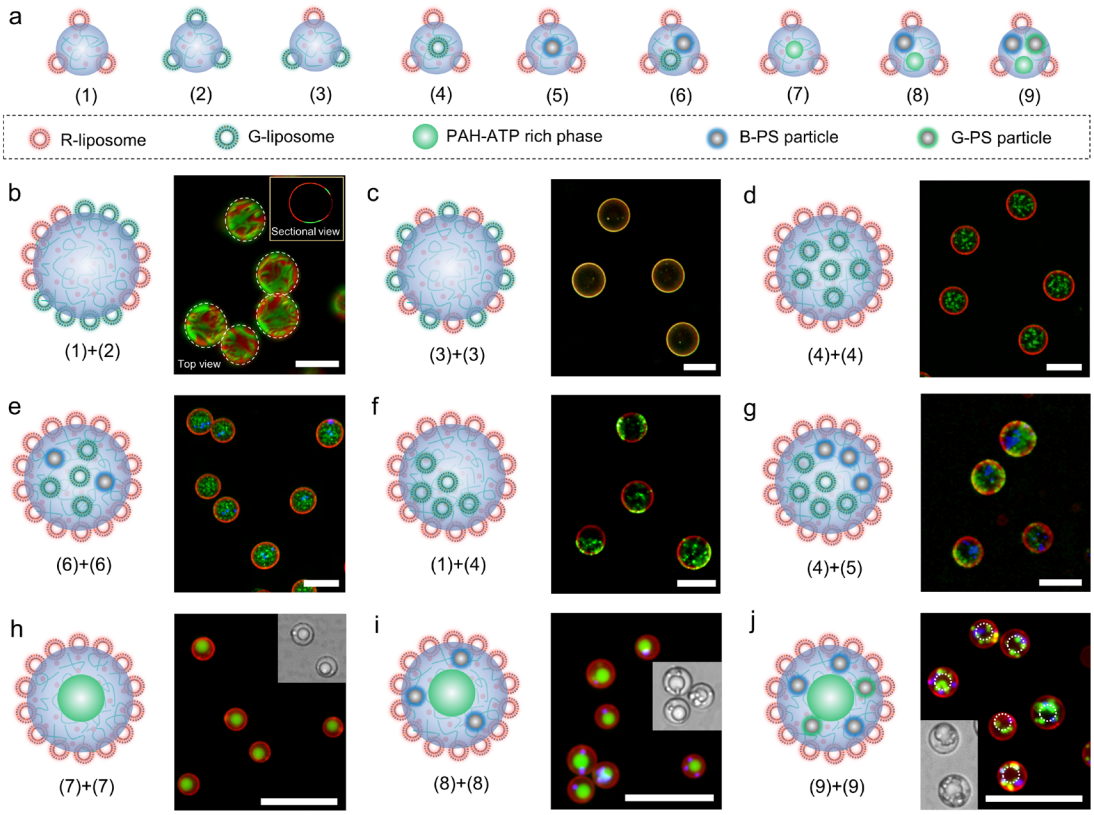

Figure 3. Engineering hierarchical coacervates via the programmable combinatorial fusion of small coacervate building blocks. a, Schematic of the nine small coacervate building blocks (1)-(9) formed via the gentle mixing of PDDA, ATP, PAH or different particles. **b** and **c**, Schematic and fluorescence images of PDDA-ATP coacervates with heterogeneously (**b**) and homogeneously (**c**) distributed red fluorescent liposome (R-liposome) and green fluorescent liposome (G-liposome) on surface formed via the vortex promoted fusion of (1) and (2) for **b** or self-fusion of (3) for **c**. **d-g**, Schematic and fluorescence images of R-liposome coated PDDA-ATP coacervates containing particles inside with different spatial organization: homogeneously distributed G-liposome (**d**) via self-fusion of (4), homogeneously distributed G-liposome and blue fluorescent PS particle (B-PS particle) (**e**) via self-fusion of (5), heterogeneously distributed G-liposome (**f**) via fusion of (1) and (4), and heterogeneously distributed G-liposome and B-PS particle (**g**) via fusion of (4) and (5). **h-j**, schematic, fluorescence images and inset bright field images of R-liposome coated phase separated coacervates (PAH-ATP rich phase inside PDDA-ATP rich phase) with no particle inside (**h**) formed via self-fusion of (7), B-PS particle in PDDA-ATP rich phase (**i**) via self-fusion of (8) or green fluorescent PS particle (G-PS particle) and B-PS particle in PDDA-ATP phase (**j**) via self-fusion of (9). The scales bars were 20 μm.

Sequential loading and volume growth of liposome stabilized coacervates. Besides the combinatorial fusion approach, the hierarchy of coacervates could also be engineered via post-loading (Fig. 4a). PDDA-ATP coacervates (φ=3/2) stabilized by DOPC/DOPS liposomes (χ=10%) are used as the starting structure to perform post-loading experiments, where the coacervates are mixed with different particles or bare coacervates, followed by subsequent vortexing for 10 s. G-PS particle and B-PS particles are shown to be sequentially loaded into the coacervates through successive vortex-mixing (Fig. 4b). The liposome-stabilized coacervates could sequester bare PAH-ATP coacervates to generate multiphase coacervates (Fig. 4c). Moreover, the liposome-coated coacervates could also sequester bare PDDA-ATP coacervates with same component, leading to

volume growth to defined size, as shown in Fig. 4d-e. The volume growth is hypothesized to be the result of a series of fusion events. Liposome coated coacervates and bare coacervates fuse when interact, resulting in volume increase and liposome coverage decrease of liposome coated coacervates, which then fuse with each other until a new liposome steric hindrance layer is established. The sequential loading into particle stabilized coacervates represents another approach to engineer hierarchical coacervates and integrate functional components into them. Furthermore, it might imply a possible predatory behavior of protocells on early Earth that particle coated coacervates engulf other particles or bare coacervates for function evolution or volume growth.

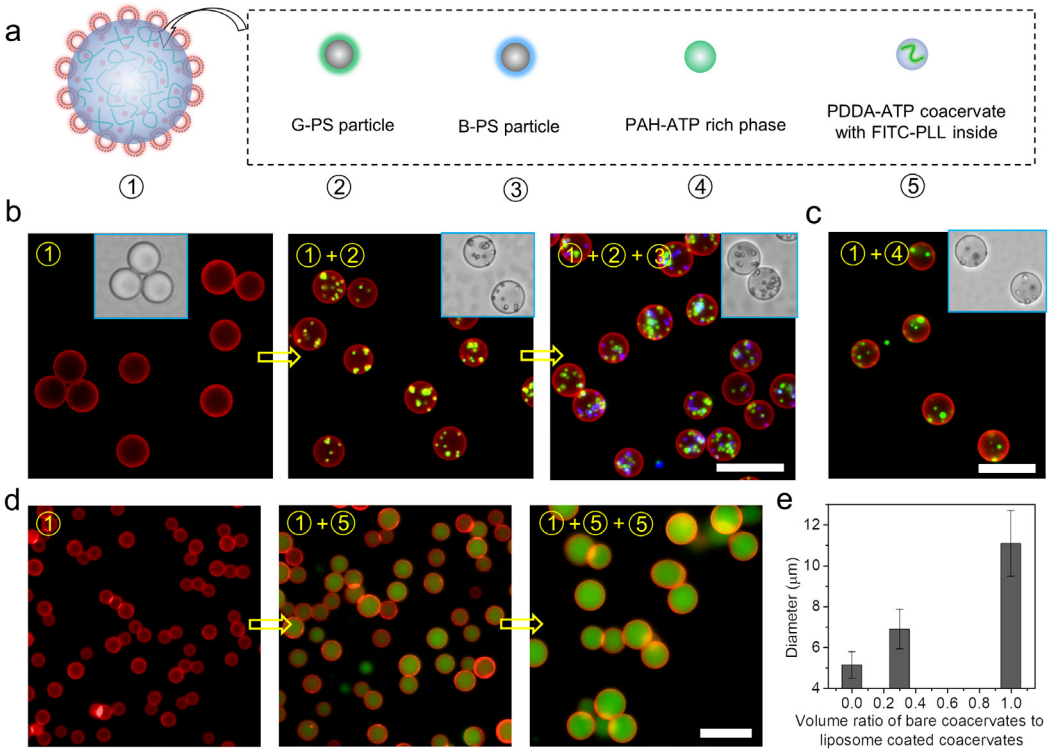

Figure 4. Sequential loading in liposome stabilized coacervates. a, Schematic illustrating the sequential loading of different materials, including G-PS particle ②, B-PS particle ③, PAH-ATP rich coacervate ④, and bare PDDA-ATP coacervate with FITC-PLL inside ⑤, into the R-liposome stabilized coacervates ①. **b**, fluorescence and inset bright field images showing the sequential loading of ② and ③ into ①. **c**, fluorescence and inset bright field images of the multiphase coacervates with PAH-ATP rich inside formed via the loading of ④ into ①. **d**, fluorescence images showing the growth of liposome stabilized coacervates via the loading of bare coacervates with 30% volume of ① (middle image) and 100% volume of ① (image at the right side). **e**, relationship of the calculated diameter of the final liposome stabilized coacervates with the volume of added bare coacervates from 100 coacervates for each event. The scales bars were 20 μm.

Programmable assembly of coacervates into tissue-like assemblages. The emergence of multicellularity represented a major transition in the evolution of life[32], which stimulated the recent trend to build synthetic multicellular systems with emergent properties from protocell entities, such as aqueous droplets in oil[33], proteinosomes[34], and liposomes[35]. However, the inherent difficulty to control adhesion of coacervates without fusion hamper the assembly of coacervats into muticellular assemblages. Here, taking advantage of the metastable hierarchical coacervates through combinatorial fusion or sequential loading, we demonstrate a method to program the assembly of

interconnected coacervate consortia via tailoring coacervate structure. Six kinds of PDDA-ATP coacervates I-VI with different spatial organization of liposomes, magnetic particles, avidin-PS particles or PAH-ATP rich phase are prepared for coacervate assemblage formation (Fig. 5a). DOPC/DOPS (χ=10%) liposome-coated coacervates (Coacervates I), DOPC/DOPS (χ=10%) liposome-coated coacervates with 1 μm magnetic particle inside (Coacervates II), and 30 nm magnetic nanoparticle-coated coacervates (Coacervates III) exhibit non-specific aggregation into irregular clusters or magnetotactic bacteria-like aligned coacervate chains with embedded magnetic particle chains (Inset in Fig. 5b) after the application of external stimuli (pH or magnetic field); the consequent aggregation of coacervates I and II is reversible (Fig.5b). Specific aggregation was observed in coacervates IV (90% DOPC+10% biotin-lipid liposome coated coacervate) and V (Avidin-PS nanoparticle coated coacervates). Coacervates IV (Red fluorescence) and 1 μm avidin-PS particles (Green fluorescence) specifically associated into coacervate assemblage containing one coacervate type (Fig. 5c). More complicated coacervate assemblage containing two coacervate types IV (Red fluorescence) and V (Green fluorescence) can be formed via the specific association of the biotin group in coacervate IV and the avidin group in coacervate V (Fig. 5d).

To form tissue-like coacervate assemblages at millimeter scale, we impose a magnetic field gradient on the top surface of a magnet (100mm×50mm×5mm) to guide the assembly of coacervates III or VI that have been coated by a mixture of magnetic nanoparticles and liposomes with different fluorescence (Lipid/Fe mass ratio=α). Strip-shaped coacervate assemblages with parallelly or serially coded patterns are generated via simultaneous or successive assembly of coacervate III (α=1/4) with respective red and green fluorescence as shown in Fig. 5f-h. Multiphase coacervates VI (α=4/1) are assembled using same method into tissue-like assemblage with excess complexity (Fig. 5i). Coacervates in the strip-shaped assemblages are interconnected and exhibit collective deformation or motion such as rotation, translation, folding and unfolding under magnetic field (Fig. S10). Moreover, diffusion-related morphology evolution is observed in coacervate III assemblage when 50 mM ATP is added from the right side of the assemblage (Fig. 5g). The high concentration of ATP induces desoprtion of the liposomes from coacervates (Inset schematic in Fig. 5g and Fig. S11). Therefore, coacervates fuse into defined size depending on α for a new magnetic particle steric hindrance layer (Inset schematic in Fig. 5g and Fig. S12). With ATP diffusion, fusion events sweep from right to left (Fig.5g). These results indicated the ability of the coacervate assemblage to exhibit collective behavior in response to physical or chemical stimuli.

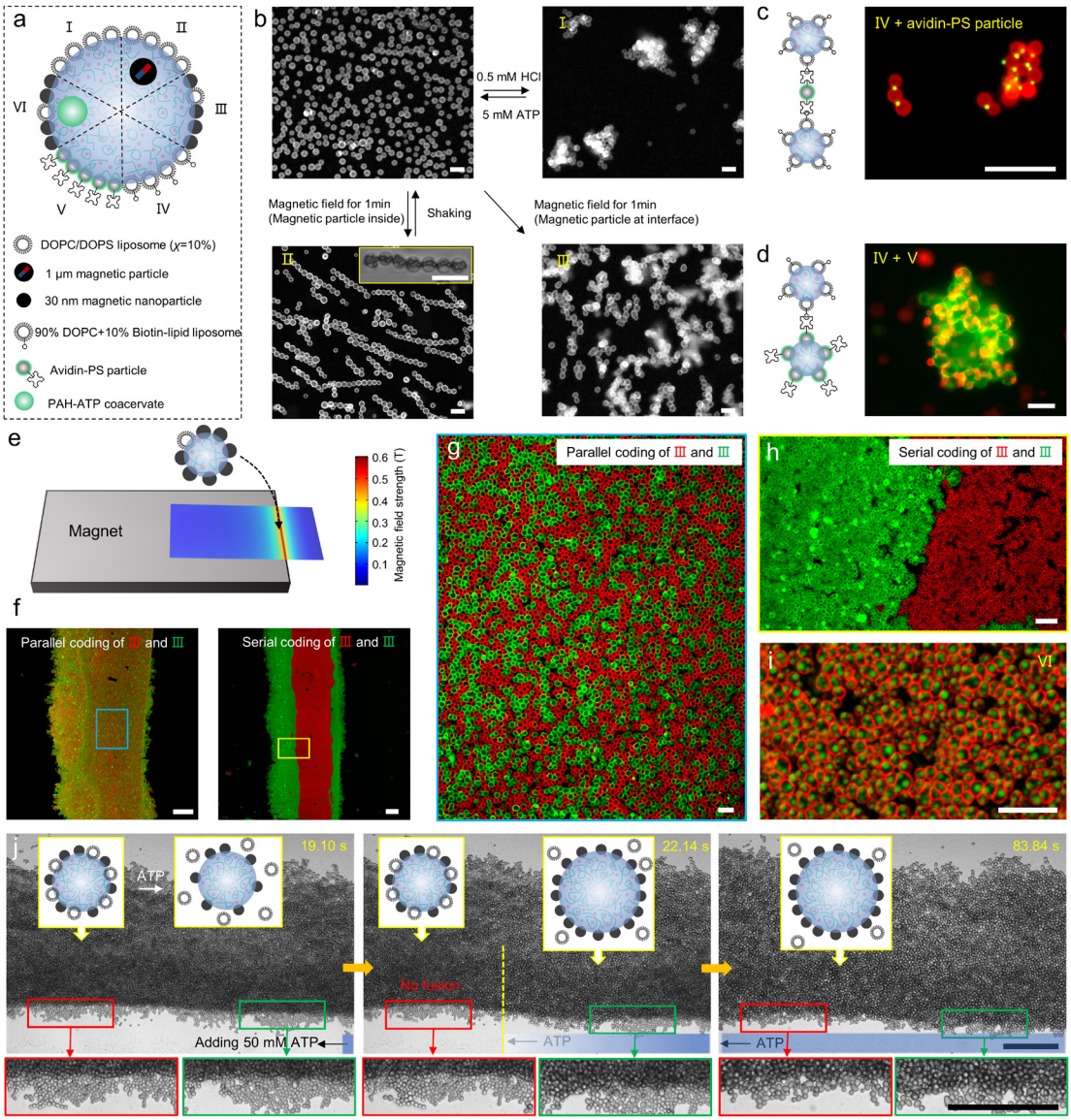

Figure 5. Assembly of coacervates into tissue-like assemblages and their collective behavior. a, Schematic of the six kinds of coacervates for coacervate assemblage formation. **b**, PDDA-ATP coacervate assemblage formation via non-specific interaction of coacervates I-III respectively. The inset was a bright field image of coacervate assemblage formed from coacervate II. **c**, Schematic and merged fluorescence image showing the specific aggregation of red fluorescent coacervate IV linked by 1μm green fluorescent avidin-PS particle. **d**, Schematic and merged fluorescence image showing the specific association of coacervates IV (red fluorescence) and V (green fluorescence). **e**, Simulated magnetic field distribution on one side of the 100mm×50mm×5mm magnet top surface. **f**, Fluorescence images of the coacervates assemblages via the parallel (left) and serial (right) coding of coacervates III with respective red and green fluorescence. **g** and **h**, Enlarged images of the parallelly (**g**) and serially (**h**) coded coacervates assemblages in the white box in **f**. **i**, Merged fluorescence image of the coacervate assemblage formed from coacervate VI. **j**, Collective fusion of coacervates III in the assemblage after the addition of 5 μL ATP stock solution from the right side of the assemblage. The inset in the left image was a schematic showing the shedding of liposomes after adding ATP. The inset in the middle and right images were schematic showing the structure of the coacervates at position directed by the arrows. The molecular ratio α of lipid and Fe was 1/1. Scale bars in **b-d** and **g-i** were 10 μm. Scale bars in **f** and **j** were 200 μm.

Unilamellar phospholipid membrane assembly on coacervates. Biological cells are bounded with phospholipid membranes separating the intracellular and extracellular space. To bridge the gap between coacervate-based protocell lacking a structural membrane and membrane bounded biological cells, a prebiotic plausible mechanism should exist for coacervates to guide the formation of a semi-permeable biological membrane. To address this, we illustrate two ways to form monodisperse giant unilamellar vesicles (GUVs) based on coacervates. The first one is demonstrated by forming monodisperse coacervates coated by 1,2-dipalmitoyl-sn-glycero-3-phosphocholine (DPPC)/DOPS (χ=2%) membrane patches firstly and then heating at 50°C to fuse the membrane patches into continuous lipid bilayer (Fig. S13). GUVs in gel phase with average diameter below 2.5 μm are generated using this method. The second way is by freeze-thaw treatment of monodisperse coacervates coated by DOPC/DOPS/Chol (37/3/10) liposomes (Fig. 6). GUVs formed using this method contain fluidic membrane more analogous to modern cell membrane according to fluorescence recovery after photobleaching (FRAP) experiments (Fig. 6c). Considering the existence of iterative freeze–thaw cycles on earth[36,37], the second method might be more plausible in forming prebiotic membrane on coacervates.

According to fluorescein permeability test, GUVs formed through freeze-thaw method displays gated permeability to fluorescein (Fig. 6b). With PDDA in dispersion media, GUVs become leaky and enrich fluorescein in coacervate nucleus, probably due to the transient membrane defects generated by PDDA adsorption. The removal of adsorbed PDDA by washing with excess 5 mM ATP solution results in blockage of the membrane permeability to fluorescein. Phospholipid membrane constituting modern cells is previously thought to be unsuitable for primitive cells, partially due to their strong hinderance for the permeability of polar molecules and thus highly evolved protein machinery is required for the transportation of nutrients or waste products[38]. The gated permeability of the coacervate-supported GUVs in this work implies the possibility of phospholipid constitution in primitive cells. Permanent permeability to fluorescein is realized in the coacervate supported GUVs by incubating the GUVs with melittin, as indicated by the right image in Fig. 6b), consistent with the anticipated unilamellarity of the phospholipid membrane. The coacervate nucleus inside the GUVs is verified by the phase contrast images (Inset in Fig. 6b) and FRAP experiment (Fig. 6d).

By using liquid nitrogen to freeze liposome-coated (L-) coacervates, monodisperse GUVs with controlled size are generated through the freeze-thaw method (Fig. 6e, f). Lipid concentration in the pre-frozen L-coacervates determines the diameter of the GUVs, which ranges from ~8 μm to ~2 μm when lipid concentration increases from 0.015 mg/mL to 0.05 mg/mL. The influence of freezing conditions (-196°C in liquid nitrogen, -80°C or -20°C) on GUVs formation is indicated in Fig. 6g and S14. The transformation efficiency from L-coacervates to GUVs decreases from ~50% to ~10% as the freezing temperature increases. Besides, larger polydispersity index of the samples is observed at higher freezing temperature (Fig. S14). When liposome particles with heterogenous lamellarity were co-assembled on coacervate surface, unilamellar vesicles are tended to be generated (Fig. S15), which indicated the ability of this freeze-thaw method to regularize heterogenous lipid assemblies towards membrane unilamellarity, a hallmark of modern cells. Membrane-coated coacervates could have enabled the generation of chemical gradient between the inside and outside of the droplet, promoting the evolution[39].

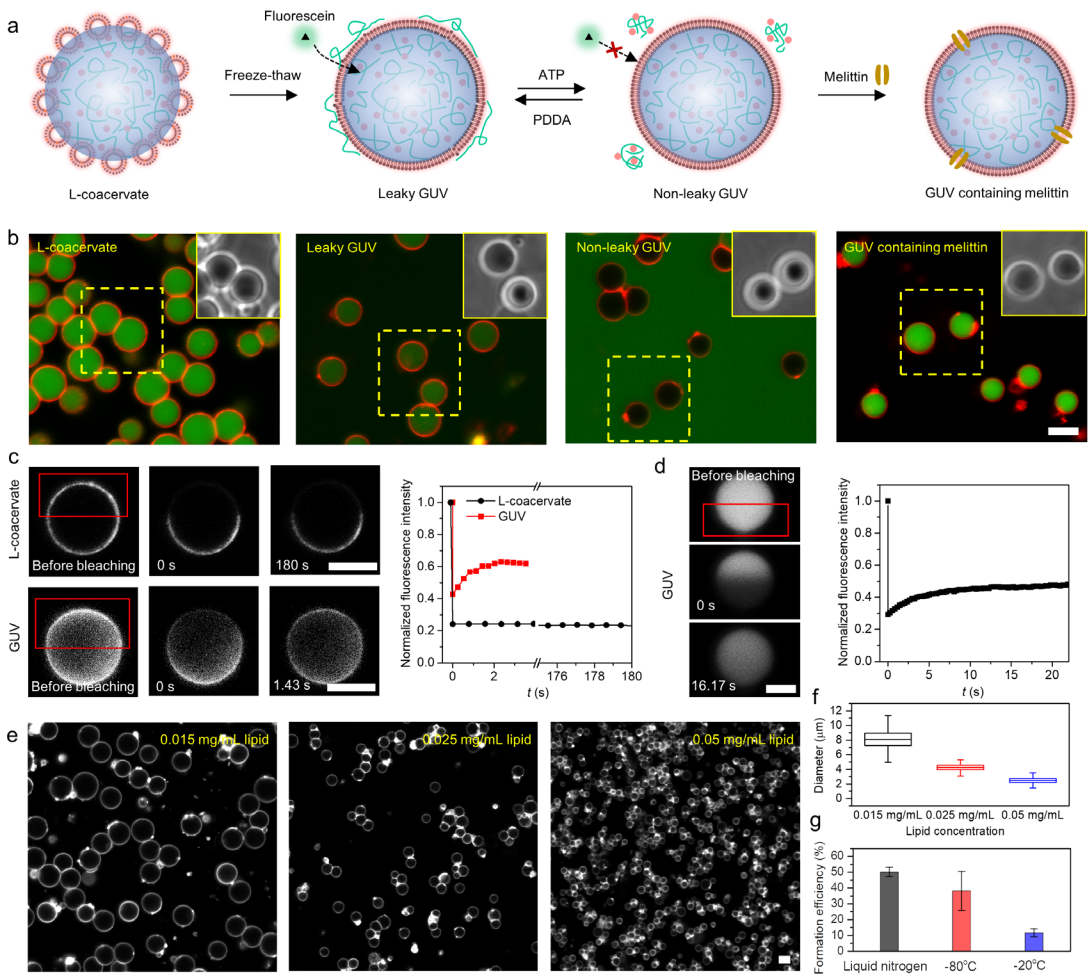

Figure 6. Unilamellar phospholipid bilayer formation on coacervates. a, Schematic illustrating the formation and permeability of unilamellar DOPC/DOPS/Chol (37/3/10) phospholipid bilayer on PDDA-ATP coacervates (φ=7/3) from liposome coated coacervates (L-coacervate). **b**, Fluorescence images showing the permeability of L-coacervate, leaky GUV, Non-leaky GUV, and GUV containing melittin to fluorescein. The inset were the phase contrast images of droplets in the yellow dash boxes. The sample was frozen in liquid nitrogen. **c**, Fluorescence recovery after photobleaching (FRAP) experiments of rhodamine-DOPE in L-coacervate and GUV. **d**, FRAP experiment of FITC-PLL inside GUV. **e** and **f**, Size control of GUVs formed via freeze in liquid nitrogen. The error bar represents the standard deviation. For all cases, n>100. **g**, Formation efficiency of GUVs from L-coacervate calculated from the turbidity change after adding NaCl at different freezing conditions. The error bar represents the standard error of mean (SEM), $n = 3$ independent experiments. The scale bars in **b**-**e** were 5 μm.

Stability and functioning of coacervate-supported GUVs at extreme environments. The stability of PDDA-ATP coacervate-supported GUVs in dispersion media with different salt concentration or pH condition was investigated via turbidity test. No turbidity change was observed for coacervate supported GUVs at NaCl concentration between 0-1.6 M and pH condition with pH value at 2 and NaOH concentration at 1 M, as shown in Fig. 7a, b. In contrary, bare PDDA-ATP coacervates dissociate when the NaCl concentration increases above 50 mM, pH value drops below 3, or the NaOH concentration increases above 100 mM. Moreover, the coacervate-supported GUVs retained spherical shape in different solution media (Fig. 7c).

Free GUVs were reported to easily deform or rupture under osmotic shock[40]. Bare coacervates are

highly sensitive to salt concentration and pH condition (Fig. 7a, b). However, coacervate-supported GUVs integrating these two components display unexpected acid-, alkali-, salt-, and osmosis-resistances. In the hybrid system, phospholipid membrane provides an effective barrier to ions and may maintain a transmembrane proton gradient[8], thus keeping the stability of the coacervate nucleus at different salt concentration and pH condition. In turn, the repulsive hydration and electrostatic forces inside coacervate nucleus render the generation of a hydrostatic pressure preventing water loss, which contributes to the osmotic stability of phospholipid vesicles. The remarkable stability of the coacervate-supported GUVs is a synergetic effect of integrating these two components.

FITC-PLL with high partition coefficient in coacervate phase (Fig. S16) is used as the probe to measure the pH value inside coacervates. The normalized fluorescence intensity I of FITC-PLL (Fluorescence intensity versus measured fluorescence intensity at pH=7) in aqueous solution and bare coacervates dispersion decreases with decreasing pH value, as shown in Fig. 7d. No obvious difference of the relationship between I and pH value is observed in these two systems (black and red lines in Fig. 7d), indicating negligible pH value difference between bare coacervates and dispersion media. A linear relationship between log(I) and pH value is observed at pH value range of 2-7, which is used to estimate pH value inside coacervate-supported GUVs based on the measured I in Fig. 7d. The coacervate nucleus keeps a pH value between 5.5 to 7 when pH value outside changed from 2 to 7 (Fig. 7e), providing a pH homeostasis and maintaining a pH gradient across the membrane. The pH homeostasis enables the functioning of coacervate-supported GUVs at extreme acidic conditions. A solution media with pH=2 is shown to denature horseradish peroxidase (HRP) in bulk solution (Black line in Fig. 7f). However, HRP inside coacervate supported GUVs dispersed in such an acid condition still preserves their catalytic ability for the transformation of amplex red to red fluorescein resorufin products (Fluorescence image and red line in Fig. 7f). The stability and the ability to retain enzyme function of coacervate-supported GUVs at extreme conditions might make them survive from the severe environment on early Earth and develop into modern cells. One possible drawback of their morphology stability might be that it leads to the difficulty for division. The implantation of non-equilibrium processes[16] or the dissociation of coacervate nucleus might address this problem. For instance, the coacervate nucleus dissociated when the coacervate-supported GUVs interact with 150 mM NaCl and 0.5 μg/mL melittin, resulting in the formation of free GUVs with active membrane fluctuations and osmosis-responsive morphology transformation into lipid tubes (Fig. S17). From these free GUVs encapsulated with highly concentrated polymers, the earliest cellular life could have emerged.

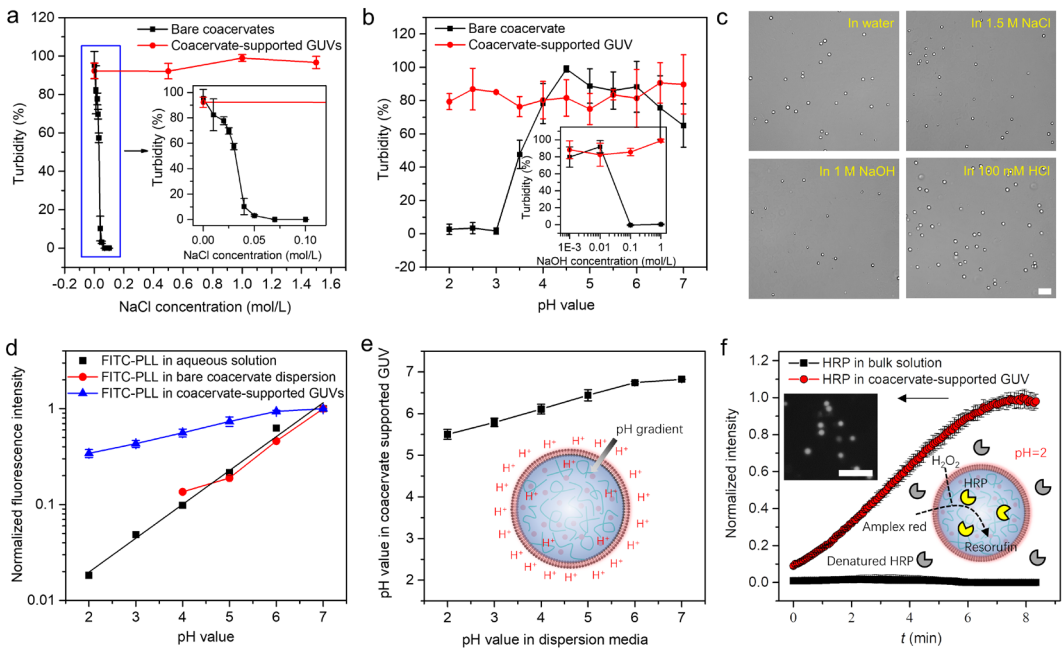

Figure 7. Stability and functioning of coacervate-supported GUVs at extreme environments. a, Turbidity test of bare coacervates and coacervate supported GUVs at different NaCl concentration. The inset was the enlarged image in blue box. **b**, Turbidity test of bare coacervates and coacervate supported GUVs at different pH condition. The inset was the turbidity test at different concentration of NaOH. **c**, Bright field images of coacervate supported GUVs in different solution media. **d**, Normalized fluorescence intensity of FITC-PLL in bare coacervates dispersion and coacervate supported GUVs. **e**, Calculated pH value in coacervate supported GUVs versus pH value in dispersion media. A pH gradient was fabricated as shown by the inset schematic. **f**, Enzyme catalyzed reaction in bulk solution and coacervate supported GUVs at pH=2. The inset was the schematic and a typical fluorescence image showing the generation of resorufin in coacervate supported GUVs. The error bars represent the standard error of mean (SEM), $n = 3$ independent experiments. The scale bars in **c** and **f** were 20 μm.

Conclusion

By assembling coacervate-forming components with colloidal particles, this work demonstrated an integrative approach for the combinatorially engineering of coacervates towards logically integrated protocell model with cellular hallmarks of size uniformity and unilamellar membransation exploiting no microfluidic devices. Hydrodynamic forcing, which generally exacerbated size distribution of an emulsion system, was found to promote the bulk-assembly of monodisperse coacervates in one minute. The limited coalescence of particle coated coacervates as well as interfacial tension mediated loading laid the foundation to combinatorially engineer the coacervates towards defined complexity. This speciation of the metastable coacervate compartments further enabled the assembly of high-order tissue-like coacervate assemblages exhibiting collective morphology evolution. Monodisperse GUVs were generated via freeze-thaw treatment of liposome particles coated coacervates, which allowed gated permeability of polar molecules without proteins and retained structural and functional integrity at extreme environments. As only electrostatic interaction is involved in vesicle assembly, this approach might also be utilized for the formation of unilamellar membrane on coacervates from other amphiphilic molecules.

Contrary to spontaneously assembled compartments with great uncertainty or low efficiency for material loading, the integrative approach in this work allowed combinatorial loading towards proto-

compartments speciation. Therefore, the probability for appropriate integration of inanimate matter towards life is remarkably increased. This integrative approach is promising used to verify theoretical models about origin of life[16,41] and the high throughput screening of possible integrated form of primitive life from a high diversity of inanimate matter. Moreover, this work can also generate monodisperse coacervates and GUVs with flexibly integrated functions for synthetic biology, biosensing, and advanced delivery systems.

References

1 Ruiz-Mirazo, K., Briones, C. & de la Escosura, A. Prebiotic Systems Chemistry: New Perspectives for the Origins of Life. *Chemical Reviews* **114**, 285-366 (2014).

2 Monreal Santiago, G., Liu, K., Browne, W. R. & Otto, S. Emergence of light-driven protometabolism on recruitment of a photocatalytic cofactor by a self-replicator. *Nature Chemistry* **12**, 603-607 (2020).

3 Szostak, J. W., Bartel, D. P. & Luisi, P. L. Synthesizing life. *Nature* **409**, 387-390 (2001).

4 Rasmussen, S. *et al.* Transitions from Nonliving to Living Matter. *Science* **303**, 963-965 (2004).

5 Schwille, P. *et al.* MaxSynBio: Avenues Towards Creating Cells from the Bottom Up. *Angewandte Chemie International Edition* **57**, 13382-13392 (2018).

6 Mansy, S. S. *et al.* Template-directed synthesis of a genetic polymer in a model protocell. *Nature* **454**, 122-125 (2008).

7 Adamala, K. & Szostak, J. W. Nonenzymatic Template-Directed RNA Synthesis Inside Model Protocells. *Science* **342**, 1098-1100 (2013).

8 Liu, L. *et al.* Enzyme-free synthesis of natural phospholipids in water. *Nature Chemistry* **12**, 1029-1034 (2020).

9 Donau, C. *et al.* Active coacervate droplets as a model for membraneless organelles and protocells. *Nature Communications* **11**, 5167 (2020).

10 Dora Tang, T. Y. *et al.* Fatty acid membrane assembly on coacervate microdroplets as a step towards a hybrid protocell model. *Nature Chemistry* **6**, 527-533 (2014).

11 Chen, I. A. & Walde, P. From self-assembled vesicles to protocells. *Cold Spring Harbor perspectives in biology* **2**, a002170 (2010).

12 Lombard, J., López-García, P. & Moreira, D. The early evolution of lipid membranes and the three domains of life. *Nature Reviews Microbiology* **10**, 507-515 (2012).

13 Zhu, T. F. & Szostak, J. W. Coupled Growth and Division of Model Protocell Membranes. *Journal of the American Chemical Society* **131**, 5705-5713 (2009).

14 Li, M., Huang, X., Tang, T. Y. D. & Mann, S. Synthetic cellularity based on non-lipid micro-compartments and protocell models. *Current Opinion in Chemical Biology* **22**, 1-11 (2014).

15 Frankel, E. A., Bevilacqua, P. C. & Keating, C. D. Polyamine/Nucleotide Coacervates Provide Strong Compartmentalization of Mg2+, Nucleotides, and RNA. *Langmuir* **32**, 2041-2049 (2016).

16 Zwicker, D., Seyboldt, R., Weber, C. A., Hyman, A. A. & Jülicher, F. Growth and division of active droplets provides a model for protocells. *Nature Physics* **13**, 408-413 (2017).

17 Brangwynne, C. P. *et al.* Germline P Granules Are Liquid Droplets That Localize by Controlled Dissolution/Condensation. *Science* **324**, 1729-1732 (2009).

18 Banani, S. F., Lee, H. O., Hyman, A. A. & Rosen, M. K. Biomolecular condensates: organizers of cellular biochemistry. *Nature Reviews Molecular Cell Biology* **18**, 285-298 (2017).

19 Jia, T. Z., Hentrich, C. & Szostak, J. W. Rapid RNA Exchange in Aqueous Two-Phase System and Coacervate Droplets. *Origins of Life and Evolution of Biospheres* **44**, 1-12 (2014).
20 Garenne, D. *et al.* Sequestration of Proteins by Fatty Acid Coacervates for Their Encapsulation within Vesicles. *Angewandte Chemie International Edition* **55**, 13475-13479 (2016).
21 Koga, S., Williams, D. S., Perriman, A. W. & Mann, S. Peptide–nucleotide microdroplets as a step towards a membrane-free protocell model. *Nature Chemistry* **3**, 720-724 (2011).
22 Pavan Kumar, B. V. V. S. *et al.* Chloroplast-containing coacervate micro-droplets as a step towards photosynthetically active membrane-free protocells. *Chemical Communications* **54**, 3594-3597 (2018).
23 Pir Cakmak, F., Grigas, A. T. & Keating, C. D. Lipid Vesicle-Coated Complex Coacervates. *Langmuir* **35**, 7830-7840 (2019).
24 Mason, A. F. *et al.* Mimicking Cellular Compartmentalization in a Hierarchical Protocell through Spontaneous Spatial Organization. *ACS Central Science* **5**, 1360-1365 (2019).
25 Spruijt, E., Sprakel, J., Cohen Stuart, M. A. & van der Gucht, J. Interfacial tension between a complex coacervate phase and its coexisting aqueous phase. *Soft Matter* **6**, 172-178 (2010).
26 Shi, S. & Russell, T. P. Nanoparticle Assembly at Liquid–Liquid Interfaces: From the Nanoscale to Mesoscale. *Advanced Materials* **30**, 1800714 (2018).
27 Song, Y. *et al.* Fabrication of fibrillosomes from droplets stabilized by protein nanofibrils at all-aqueous interfaces. *Nature Communications* **7**, 12934 (2016).
28 Milovanovic, D., Wu, Y., Bian, X. & De Camilli, P. A liquid phase of synapsin and lipid vesicles. *Science* **361**, 604-607 (2018).
29 Ridel, L., Bolzinger, M.-A., Gilon-Delepine, N., Dugas, P.-Y. & Chevalier, Y. Pickering emulsions stabilized by charged nanoparticles. *Soft Matter* **12**, 7564-7576 (2016).
30 Masschaele, K., Park, B. J., Furst, E. M., Fransaer, J. & Vermant, J. Finite Ion-Size Effects Dominate the Interaction between Charged Colloidal Particles at an Oil-Water Interface. *Physical Review Letters* **105**, 048303 (2010).
31 Bizmark, N. & Ioannidis, M. A. Nanoparticle-stabilised emulsions: droplet armouring vs. droplet bridging. *Soft Matter* **14**, 6404-6408 (2018).
32 Grosberg, R. K. & Strathmann, R. R. The Evolution of Multicellularity: A Minor Major Transition? *Annual Review of Ecology, Evolution, and Systematics* **38**, 621-654 (2007).
33 Villar, G., Graham, A. D. & Bayley, H. A Tissue-Like Printed Material. *Science* **340**, 48-52 (2013).
34 Gobbo, P. *et al.* Programmed assembly of synthetic protocells into thermoresponsive prototissues. *Nature Materials* **17**, 1145-1153 (2018).
35 Li, Q., Li, S., Zhang, X., Xu, W. & Han, X. Programmed magnetic manipulation of vesicles into spatially coded prototissue architectures arrays. *Nature Communications* **11**, 232 (2020).
36 Bada, J. L., Bigham, C. & Miller, S. L. Impact melting of frozen oceans on the early Earth: Implications for the origin of life. *Proceedings of the National Academy of Sciences* **91**, 1248-1250 (1994).
37 Attwater, J., Wochner, A., Pinheiro, V. B., Coulson, A. & Holliger, P. Ice as a protocellular medium for RNA replication. *Nature Communications* **1**, 76 (2010).
38 Budin, I. & Szostak, J. W. Expanding Roles for Diverse Physical Phenomena During the Origin of Life. *Annual Review of Biophysics* **39**, 245-263 (2010).
39 Budin, I. & Szostak, J. W. Physical effects underlying the transition from primitive to modern

cell membranes. *Proceedings of the National Academy of Sciences* **108**, 5249-5254 (2011).
40 Zong, W. *et al.* A Fissionable Artificial Eukaryote-like Cell Model. *Journal of the American Chemical Society* **139**, 9955-9960 (2017).
41 Lancet, D., Zidovetzki, R. & Markovitch, O. Systems protobiology: origin of life in lipid catalytic networks. *Journal of The Royal Society Interface* **15**, 20180159 (2018).
42 Olson, F., Hunt, C. A., Szoka, F. C., Vail, W. J. & Papahadjopoulos, D. Preparation of liposomes of defined size distribution by extrusion through polycarbonate membranes. *Biochimica et Biophysica Acta (BBA) - Biomembranes* **557**, 9-23 (1979).
43 Mason, J. T., Cunningham, R. E. & O'Leary, T. J. Lamellar-phase polymorphism in interdigitated bilayer assemblies. *Biochimica et Biophysica Acta (BBA) - Biomembranes* **1236**, 65-72 (1995).

Methods

Materials

1,2-dioleoyl-*sn*-glycero-3-phosphocholine (DOPC), 1,2-dioleoyl-*sn*-glycero-3-phospho-L-serine (sodium salt) (DOPS), 1,2-dioleoyl-*sn*-glycero-3-phosphate (sodium salt) (DOPA), 1,2-dipalmitoyl-*sn*-glycero-3-phosphoethanolamine-N-(cap biotinyl) (sodium salt) (Biotin-lipid), 1,2-dioleoyl-3-trimethylammonium-propane (chloride salt) (DOTAP), 1,2-dipalmitoyl-*sn*-glycero-3-phosphocholine (DPPC), 1,2-dipalmitoyl-sn-glycero-3-phosphoethanolamine-N-(7-nitro-2-1,3-benzoxadiazol-4-yl) (ammonium salt) (NBD PE), and 1,2-dioleoyl-*sn*-glycero-3-phosphoethanolamine-N-(lissamine rhodamine B sulfonyl) (ammonium salt) (Rhodamine PE) were purchased from Avanti Polar Lipids (USA). Poly(diallyldimethylammonium chloride) solution (PDDA, average M_w<100 kDa, 35% wt.% in water), Poly(ethyleneimine) solution (PEI, M_w~750 kDa, 50% (w/v) in water), Poly(allylamine hydrochloride) (PAH, M_w~17500), Poly(acrylic acid) (PAA, M_w~1800), Adenosine 5′-triphosphate disodium salt hydrate (ATP), Adenosine 5′-diphosphate sodium salt (ADP), Fluorescein isothiocyanate (FITC) labelled Poly-L-lysine (FITC-PLL), Poly(FITC allylamine hydrochloride) (FITC-PAH), iron oxide(II,III) magnetic nanoparticles solution (30 nm, carboxylic acid functionalized), amine-modified polystyrene (PS) nanoparticle (100 nm, fluorescent orange), cholesterol, ethanol, hydrochloric acid, sodium hydroxide, sodium chloride, glucose, sodium oleate, and fluorescein were purchased from Sigma. Horseradish peroxidase (HRP) was bought from Solarbio. QuantaRed™ enhanced chemifluorescent HRP substrate kit was purchased from ThermoFisher Scientific. Streptavidin coated PS nanoparticle (100 nm), streptavidin coated PS microparticle (1 μm), 50 nm PS-COOH nanoparticle (fluorescent dragon green), 0.5 μm PS-COOH nanoparticle (fluorescent dragon green), and 1 μm PS-COOH nanoparticle (fluorescent glacial blue) bought from Bangs Laboratories, Inc. Dynabeads™ MyOne™ Carboxylic Acid 1 μm magnetic particle was from Invitrogen. 100 nm silica particle was from Nanjing Nanorainbow Biotechnology Co., Ltd. Ag nanowire (30 nm diameter) was from Nanjing XFNANO Materials Tech Co., Ltd. 75 nm diameter PS-COOH nanoparticle (fluorescent green) was from BaseLine ChromTech Research Centre (China). Millipore Milli-Q water with a resistivity of 18.2 MΩ cm was used in the experiments.

The following stock solutions were prepared in water for coacervates formation: PDDA (50 mM, pH 7), PEI (50 mM, pH 7), ATP (50 mM, pH 7), ADP (50 mM, pH 7), PAA (50 mM, pH 7), PAH (50 mM, pH ~3). Liposomes of various compositions were formed through an extrusion

method.[42] 1 mg phospholipid mixture was dried in a centrifuge tube. 1 mL of water was then added and vortexed. The mixture was extruded through polycarbonate filter with 100 nm pore size back and forth for 11 times. The composition of the liposomes was controlled by varying the ratio of different components in the phospholipid mixture. 0.2 wt% Rhodamine PE or NBD PE were incorporated for visualization under fluorescence microscope. Lipid bilayer coated silica particles were prepared via the incubation of liposomes (1 mg lipid) with 2 mg 100 nm silica particles in ultrasonic bath for 1h and subsequent removement of free liposomes via centrifugation. 30 nm magnetic particles, 1 μm magnetic particles and 30 nm diameter Ag nanowires were used as obtained. Other particles were diluted to 1mg/mL before use.

Assembly of colloids-PDDA/ATP coacervates hybrid system

A co-assembly method was employed to fabricate the colloids-coacervate hybrid system. PDDA stock solution of volume V_1, colloidal particle dispersion of volume V_2, and water of volume V_3 were firstly mixed, and subsequently then with ATP stock solution of volume V_4 via vortex for 30 s to form coacervates. The total volume of the final mixture was 100 μL. $V_1 + V_4$ was 10 μL. The molecular ratio of PDDA and ATP φ was determined by V_1/V_4. The influences of particle types (liposomes, PS particles, silica particles, magnetic particles, or Ag nanowires), liposome concentration and PDDA/ATP ratio φ were investigated. Assembly results were characterized by fluorescence microscope.

Assembly of liposomes with other coacervate formation species

The assembly of particles with another four cationic specie-anionic specie pairs, namely, PDDA with two anionic species, ADP and PAA, and ATP with two cationic species, PAH and PEI, were investigated. DOPC/DOPS liposomes were taken as particle model. The stock solution of cationic specie, liposomes, water, and stock solution of anionic specie were mixed via vortex. The volume of the final mixture was 100 μL. For PDDA-ADP pair, the influence of PDDA/ADP molecular ratio φ(PDDA/ADP) and DOPS percentage χ in DOPC+DOPS liposomes were investigated. The sum concentration of PDDA and ADP in the final mixture was fixed at 5 mM. Liposome concentration was 0.10 mg/mL. For the assembly of PDDA-PAA pair with DOPC/DOPS (χ=50%) liposomes, the influences of NaCl concentration and PDDA/PAA molecular ratio φ(PDDA/PAA) were investigated. The sum concentration of PDDA and PAA was 20 mM. Liposome concentration was 0.10 mg/mL. For the assembly of PAH-ATP pair with DOPC/DOPS (χ=10%) liposomes, the influences of pH value in the final mixture and PAH/ATP molecular ratio φ(PAH/ATP) were investigated. [PAH]+[ATP] concentration was 25 mM. Liposome concentration was 0.10 mg/mL. For the assembly of PEI-ATP pair with DOPC/DOPS (χ=10%) liposomes, the influence of pH value in the final mixture and PEI/ATP ratio φ(PEI/ATP) were investigated. [PEI]+[ATP] concentration was 10 mM. Liposome concentration was 0.05 mg/mL. The assembly results were characterized using fluorescence microscope and organized as phase diagrams.

Hierarchical coacervates formation via combinatorial fusion

A series of coacervate precursors as building blocks were prepared via the firstly mixing of PDDA with liposomes, other colloidal particles, or PAH, and then the gentle mixing with ATP. Three kinds of liposomes, including DOPC/DOPS (χ=10%) liposome with red fluorescence, DOPC/DOPS (χ=10%) liposome with green fluorescence and DOPC/DOPS (χ=50%) liposome with green

fluorescence, and two kinds of PS particles, including 0.5 μm PS-COOH particle with green fluorescence and 1 μm PS-COOH particle with blue fluorescence were used in the experiment. Nine types of building blocks were prepared, including coacervate coated by liposome with red fluorescence (R-liposome) (1), coacervate coated by liposome with green fluorescence (G-liposome) (2), coacervate coated by homogeneous mixture of R-liposome and G-liposome (3), coacervate coated by R-liposome with G-liposome inside (4), coacervate coated by R-liposome with blue fluorescent PS particle (B-PS particle) inside (5), coacervate coated by R-liposome with G-liposome and B-PS particle inside (6), coacervate coated by R-liposome with PAH-ATP rich phase inside (7), coacervate coated by R-liposome with B-PS particle and PAH-ATP rich phase inside (8), and coacervate coated by R-liposome with G-liposome, B-PS particle and PAH-ATP rich phase inside (9). The volume of each coacervate building block dispersion was 100 μL. The total concentration of cationic species was 3 mM. ATP concentration was 2 mM. The total concentration of DOPC/DOPS (χ=10%) liposome was 0.015 mg/mL in each coacervate building block dispersion. These building blocks were combinatorically mixed and then vortexed for 30 s to generate coacervates with different hierarchical structures.

Phagocytosis-mimic sequential loading and coacervate volume growth

DOPC/DOPS (χ=10%) liposomes stabilized PDDA-ATP coacervates (φ=3/2) were formed via vortex. 0.5 μm PS-COOH particle with green fluorescence, 1 μm PS-COOH particle with blue fluorescence, bare PAH-ATP coacervates (φ(PAH/ATP) =1/1) with FITC-PAH inside or bare PDDA-ATP coacervates (φ=3/2) with FITC-PLL inside were added in the liposomes stabilized coacervates dispersion. The mixture was then vortexed for 10 seconds. The positioning of particles or bare coacervates and the volume variation of the liposomes stabilized coacervates were characterized using the fluorescence microscope.

Assembly of coacervates into tissue-like coacervates assemblages

Six kinds of coacervates with different components at interfaces or inside were prepared via vortex, including DOPC/DOPS (χ=10%) liposomes coated PDDA-ATP coacervates (φ=3/2) without (I) or with (II) 1 μm magnetic particle inside, PDDA-ATP coacervates coated by mixture of 30 nm magnetic particles and DOPC/DOPS (χ=10%) liposomes without (III) or with (φ(PDDA/PAH/ATP)=1/1/2) (VI) PAH-ATP rich phase inside, 90% DOPC+10% biotin-lipid liposome coated coacervate (φ=3/2) (IV), and 100 nm avidin-PS particle coated coacervates (φ=3/2) (V). These six kinds of coacervates were taken as building blocks to fabricate tissue-like coacervates assemblages through non-specific or specific association. External stimulus, such as pH value, ATP concentration or magnetic field, were used to guide the assembly. The specific association of coacervates IV or V was carried out by the gentle shaking of the mixture of coacervate IV and 1 μm avidin-PS particle or the mixture of coacervate IV and V on a shaking table for 1 h. To form coacervate assemblages from massive coacervates with defined morphology and spatial organization, the gradient magnetic field at the edge of the magnet top surface was utilized to guide the assembly of magnetic nanoparticles stabilized coacervates III and VI. A coverslip was placed on one side of the top surface of the magnet (100mm×50mm×5mm). Dispersions of magnetic nanoparticles stabilized coacervates were then simultaneously or successively placed on the coverslip to allow the formation of belt-shaped coacervate assemblages guided by magnetic field. Magnetic field distribution was simulated using the COMSOL Multiphysics 4.4 software.

Unilamellar phospholipid bilayer formation on coacervates

Two ways were employed to generate unilamellar phospholipid bilayer on coacervate surface. The first way was based on the firstly formation of coacervates coated by lipid bilayer fragments and the subsequent fusion of these fragments into continuous phospholipid membrane. 8 μL PDDA stock solution and (190 μL - V_{lipid}) H_2O were firstly mixed, and then with V_{lipid} of DPPC/DOPS (molecular ratio=49/1) via vortex for 10s to generate lipid bilayer fragments.[43] Monodisperse coacervates (Coacervates M1) were obtained by the further mixing of the above mixture with 2 μL ATP stock solution. The transformation of coacervate M1 to coacervates M2 encompassed by continuous membrane was realized by heating the sample at 50°C for 10 min. The transformation efficiency was calculated by measuring the turbidity change of the heating treated sample before and after the addition of NaCl solution to dissolve unprotected coacervates from membrane. Coacervate M2 encapsulated with 100 nm liposomes was generated by the addition of 1 μL liposome dispersion (1 mg/mL) during the process to form coacervate M1. The permeability of coacervates were checked under fluorescence microscope by using fluorescein as a fluorescent probe. The unilarmellarity of the phospholipid membrane was verified by incubating the membrane with 5 μg/mL melittin and the subsequent permeability test to fluorescein.

The second way was based on the rupture and fusion of 100 nm liposomes on coacervates surface during a freeze and thaw process. Monodisperse PDDA-ATP Coacervates (φ=7/3) coated by DOPC/DOPS/Chol (molecular ratio=37/3/10) liposomes (L-coacervates) was formed via the vortex forced co-assembly process. The L-coacervates were frozen under liquid nitrogen, -80°C or -20°C and then thaw at room temperature to generate phospholipid membrane coated coacervates. To generate monodisperse GUVs, coacervates formed in solution with liposome concentration of 0.025 mg/mL and 0.05 mg/mL were diluted for three times before freezing. Membrane formation efficiency, permeability, and unilamellarity were checked using the same methods as the first membrane formation way. The fluidity of membrane and inner coacervate phase were characterized through fluorescence recovery after photobleaching (FRAP) experiments. The size of the coacervate-GUVs depended on the amount of nanosized liposomes that were used.

Stability and function of phospholipid membrane coated coacervates at extreme environments

The stability of the phospholipid membrane coated coacervates at different NaCl concentration and pH condition were checked by turbidity test. The images of membrane coated coacervates at different extreme environments were taken by the microscope. FITC-PLL was used as fluorescent probe to measure the pH value inside the membrane coated coacervates. Before the test, a standard curve for the normalized fluorescence intensity (measured fluorescence intensity/the measured fluorescence intensity at pH=7) of fluorescein at different pH value in bulk solution or bare coacervates dispersion was obtained by a multi-mode microplate reader. The pH value inside the membrane coated coacervates were calculated from the measured fluorescence intensity (normalized with the measured fluorescence intensity at pH=7) at different pH condition according to the standard curve. To evaluate the ability of the membrane coated coacervates to function at extreme environment, HRP was co-assembled with PDDA, ATP, and liposomes to form membrane coated coacervates encapsulated with HRP using the freeze-thaw method. The concentration of HRP in the dispersion was 0.5 U/mL. These membrane coated coacervates containing HRP were then dispersed in solution media with pH value = 2 and incubated for 60 min. The catalytic ability of

HRP in the dispersion was checked by the quantaRed™ enhanced chemifluorescent HRP substrate kit using multi-mode microplate reader. As control, the catalytic ability of HRP (0.5 U/mL) in solution with pH=2 was also checked using same method.

Characterization

The fluorescence and bright field images were taken by Leica DMIL, LED, Fluo fluorescence microscopy, Zeiss Axio Observer A1 fluorescence microscope and Zeiss LSM710 laser confocal microscope. Zeta-potential of liposomes, particles, and liposome coated PDDA-ATP coacervates were measured using Zetasizer Nano Z (Malvern Instruments, UK). The pH value was measured using the PHSJ-3F pH meter from Shanghai INESA Scientific Instrument Co., Ltd. The turbidity and fluorescence intensity were measured in 96-well plates by SpectraMax iD3 Multi-Mode Microplate Reader (Molecular Devices, CA). The turbidity was calculated by measuring the absorbance at λ=500 nm. The fluorescence intensity of fluorescein at 516 nm was collected at excitation wavelength of 470 nm. The fluorescence intensity of resorufin at 590 nm was collected at excitation wavelength of 550 nm.